Liquid−Liquid Phase Separation and Microscopic Structure in Rubidium−Ammonia Solutions Observed Using X-ray Absorption Spectroscopy

Jonathan C. Wasse,* Shusaku Hayama,† and Neal T. Skipper

Department of Physics and Astronomy, University College London, Gower Street, London, WC1E 6BT, United Kingdom

Daniel Morrison‡

Department of Chemistry, University College London, 20 Gordon Street, London, WC1H 0AJ, United Kingdom

Daniel T. Bowron

ISIS Facility, Rutherford Appleton Laboratory, Chilton, Didcot, OXON OX11 0QX, United Kingdom

Received: April 25, 2003; In Final Form: September 29, 2003

The phase behavior and microscopic structure of rubidium−ammonia ($Rb-NH_3$) solutions have been measured below the consolute temperature ($T_C = 209$ K), using the extended X-ray absorption fine structure (EXAFS) technique. The use of an X-ray video camera provides us with the first direct evidence for liquid−liquid-phase separation of metallic (concentrated) and nonmetallic (dilute) $Rb-NH_3$ solutions. Our real-time X-ray imaging also gives an extraordinary glimpse of the dynamic nature of the interior liquid−liquid interface, from which bubbles of ammonia vapor "boil" without disturbing the external meniscus. Analysis of the EXAFS structure measured above the Rb K-edge absorption at ∼15.2 keV shows that the first solvation sphere of the cation is relatively broad, with ∼6.4 N atoms being located at a distance of 2.9−3.5 Å. The location of the K-edge absorption for our solution is comparable with that measured for solid rubidium oxide, which is consistent with a Rb valency of +1 in our solution.

Introduction

Ever since their discovery by Davy in the early years of the nineteenth century[1] (previously attributed to Weyl), alkali-metal−ammonia solutions have been topics of major interest to chemists and physicists alike.[2] The generic novel properties of these metastable "metal solutions" have been well-documented and include a concentration-induced metal−nonmetal transition, extreme chemical reactivity, and very low density and viscosity. On the microscopic scale, the electronic (and, indeed, ionic) species present in these solutions are correspondingly exotic. For example, magnetic resonance experiments have identified isolated polarons, spin-paired bipolarons, truly delocalized (itinerant) electrons, and excitonic alkali atoms and anions.[1−3] Our current challenge is to understand this fascinating behavior, in terms of the microscopic structure.

Recent experiments using high-intensity X-ray and neutron scattering facilities have begun to build a detailed picture of the structure in alkali-metal−ammonia solutions.[4−11] Much of this previous work has centered on solutions of lithium, which are the least reactive of the series. Lithium is strongly solvated by ammonia and avidly forms $Li(NH_3)_4^+$. Formation of this species separates the metal cation from its excess electron and results in strong short- and intermediate-range order. This immediately raises the question of how the structure develops as the ionic size is increased and the ionic solvation weakens.

Neutron diffraction and computer modeling studies of sodium−ammonia and potassium−ammonia solutions point toward a progressive weakening of the cation solvation, and systematic loss of the diffraction pre-peak that is associated with intermediate-range order.[11−14] Nevertheless, the phase diagrams are qualitatively similar to that of lithium−ammonia ($Li-NH_3$).[2] In particular, the metal−nonmetal transition still occurs at metal concentrations of ∼4 mol % metal (4 MPM), which, for rubidium, corresponds to an atomic fraction of ∼1.03%. For these metals, the metal−nonmetal transition is accompanied by a striking liquid−liquid phase separation, in which the bright gold concentrated (metallic) solution floats on the dark-blue dilute (nonmetallic) solution. To understand this rather counterintuitive density effect, recall that the solvated excess electron has a radius of ∼3 Å,[1] and that electronic volume is therefore much greater than the electrostriction of solvent around the cation.

This imiscibility of metallic and nonmetallic metal−ammonia solutions was first observed by Kraus in 1907[15] and has since captured the imagination of many scientists. One of the earliest theoretical considerations of this separation, made by Pitzer in 1958,[16] considered the phenomenon to be analogous to liquid−vapor separation in a pure metal. Mott,[17] and more recently, Edwards and Sienko,[18] have indicated an inextricable general link between the liquid−liquid phase separation and the change of electronic configuration associated with the metal−nonmetal transition. This hypothesis is consistent with the previous EXAFS data of Acrivos and co-workers.[19]

* Author to whom correspondence should be addressed. E-mail: j.wasse@ucl.ac.uk.

† Current address: Physics Department, King's College London, Strand, London WC2R 2LS, UK.

‡ Current address: Cavendish Laboratory, University of Cambridge, Madingley Road, Cambridge, CB3 0HE, UK.

10.1021/jp0305133 CCC: $25.00 © 2003 American Chemical Society
Published on Web 12/03/2003

At this juncture, we also remind the reader that, at concentrations just below the metal−nonmetal transition, the dominant electronic species is spin-paired and bipolaronic. In contemporary literature, the existence of a miscibility gap has therefore led to analogies with the superconducting region that is found in the phase diagram for layered cuprates.[20] In this context, it is also timely to revisit the suggestion by Ogg, that rapid cooling (quenching) through the miscibility gap can lead to the formation of homogeneous superconducting metal−ammonia solids.[1,21]

Several intriguing questions and opportunities therefore arise when one considers the rubidium−ammonia ($Rb-NH_3$) system. These solutions are aggressively reactive and, therefore, are studied much less than their lower-alkali counterparts. However, rubidium will be much less strongly solvated than lithium and sodium: the ionic radii of Li^+ and Rb^+ are 0.59 and 1.61 Å, respectively,[22] and previous EXAFS studies have been interpreted in terms of an Rb−N atomic distance of ∼3.1 Å.[19] Therefore, one would expect the intermediate-range order observed in lower-alkali-metal−ammonia solutions, on the basis of correlations among solvated cations, to be absent in $Rb-NH_3$. In this case, phase separation in $Rb-NH_3$ solutions would have unambiguous origins in the metal−nonmetal transition. In this context, we recall that analysis of the critical scattering of sodium−deuterioammonia ($Na-ND_3$) shows a crossover from critical to mean field exponents, as one moves away from the critical temperature (T_C), and the concomitant correlation length for fluctuations (ξ) decreases from ∼300 Å to 10 Å.[4,5] We also note in passing that this phase separation is very isotope-sensitive. For example, $T_C = 241$ K for $Na-ND_3$ and $T_C = 231$ K for $Na-NH_3$.[2]

First, therefore, it is essential to establish whether a liquid−liquid phase separation does indeed occur in $Rb-NH_3$: such separation has never been seen visually and, indeed, is known to be absent in cesium−ammonia ($Cs-NH_3$).[2] However, conductivity studies of $Rb-NH_3$ provide some evidence for phase separation at <205 K, with boundaries at values slightly greater than 2 and 8 MPM at ∼195 K, which is the temperature at which ammonia freezes out of solution.[23] A miscibility gap in $Rb-NH_3$ has also been inferred indirectly from previous EXAFS microstructural measurements that were made by Acrivos and co-workers.[19]

In this paper, we present direct evidence for phase separation in $Rb-NH_3$ solutions at <209 K, using X-ray absorption techniques in conjunction with X-ray video imaging. In addition to this observation, we used the extended X-ray absorption fine structure (EXAFS) technique to determine the local coordination environment around rubidium in the nonmetallic region of the phase-separated solution. Furthermore, we confirm that the valence state of Rb is +1 in these solutions, which indicates full release of the valence (excess) electron into solution.

Experimental Methodology

In an X-ray absorption spectroscopy (XAS) experiment, the X-ray absorption coefficient (μ) is measured from the ratio of the intensity of the incident (monochromatic) and transmitted X-ray beams (I_0 and I, respectively), as given in eq 1:

$$\mu(E)d = \ln\left(\frac{I_0(E)}{I(E)}\right) \tag{1}$$

where d is the sample thickness. By tuning the incident photon energy, it is possible to pass through an inner shell absorption edge that is particular to one of the atomic species present. At such an edge, the radiation is absorbed and a core electron is ejected to the continuum. At energies a few tens of electron volts to a few hundreds of electron volts above the absorption edge, the photoelectrons are weakly scattered, and the interference effects between the photoelectronic waves and those waves backscattered by its neighbors results in modulations in the X-ray absorption coefficient. This is the origin of the EXAFS signal, $\chi(k)$, which is defined by the relation

$$\chi(E) = \frac{\mu(E) - \mu_0(E)}{\mu_0(E)} \tag{2}$$

where $\mu_0(E)$ is the absorption coefficient of an isolated atom. The photoelectron momentum (k) is given by

$$k = \frac{\sqrt{2m(E - E_0)}}{\hbar} \tag{3}$$

Here, m is the mass of the photoelectron, E is the X-ray photon energy, E_0 is the energy of the absorption edge, and $\hbar$ is Planck's constant divided by 2π. The EXAFS signal provides local structural information that pertains to the absorbing atom. For a review on using the EXAFS technique to study liquid structures, see the work by Filipponi.[24]

The EXAFS experiments were performed using the BM29 instrument at the European Synchrotron Radiation Facility in Grenoble, France.[25] An established technique of preparing the samples in situ was applied, using high-purity chemicals, namely, anhydrous NH_3 and rubidium (Aldrich). Because of the corrosive nature of the solution samples, the sample containers were made from high-density polyethylene cells. Preweighed pieces of the metal were handled in a dry inert argon atmosphere (O_2 content of <10 ppm and H_2O content of <10 ppm) and loaded into a cell of varying sample thickness along its length, with the thickness increasing from 1 mm to 2 mm and 3 mm for every 3 mm of height. The cell was attached to the cryostick, through a length of the inert plastic tubing. In turn, the cryostick contained a gas-feed capillary that was connected to a stainless-steel gas rig. A measured volume of ammonia was then condensed onto the metal from this gas rig at 230 K. The experiment was comprised of the measurement of the solution sample in the cell at various sample concentrations and temperatures. EXAFS measurements were made above the Rb K-edge, which is located at ∼15 keV, using a Si(311) double-crystal monochromator. The absorption spectra were recorded in transmission mode using argon-filled ionization chambers over the energy range of 14.95−15.60 keV. Intervals of ∼5, 0.26, and 1−2 eV were used for the pre-edge, edge, and EXAFS regions, respectively, with a time step of 0.5 s. A solid sample of rubidium oxide (Rb_2O) was used as the reference sample.

The data analysis was made using the GNXAS suite of programs.[26] This package is based upon multiple scattering calculations and a rigorous fitting procedure of the raw experimental data, which allowed for the fitting of two-body and many-body correlations to the experimental data. The parameters E_0 and S_0^2, which represent the absorption edge energy and reduction parameter, respectively, that were used in the analysis of the $Rb-NH_3$ solution sample were obtained for the Rb_2O reference sample, using known crystalline structural parameters.[27] Crystal structure parameters determined by Bohger and co-workers for rubidium amide ($RbND_2$) were used as the model to obtain the nearest-neighbor Rb−N distances and coordination numbers for the $Rb-NH_3$ solution.[28]

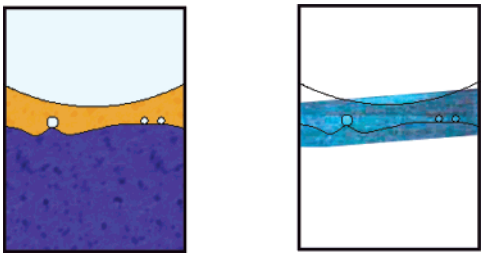

Figure 1. Liquid−liquid interface, as observed using the X-ray camera. The right-hand image shows a snapshot of the phase separation captured by an X-ray imaging camera of the sample, with the meniscus and interface marked to guide the eye. The thin horizontal line in the right-hand image at a height corresponding to the top of the bubbles marks a step in the polyethylene cell. For clarity, the colored schematic (left) highlights the two-phase region observed in the opposite photograph, i.e., the metallic (gold) and nonmetallic (blue) regions. The upper meniscus, liquid−liquid interface, and ammonia bubbles forming at the interface are shown. The width of the sample container is 1 cm.

Results and Discussion

The use of an in-line X-ray imaging video camera on the BM29 instrument allowed the authors to watch the in situ dissolution of the rubidium in liquid ammonia. Furthermore, by tuning the instrument to rubidium absorption, we were able to obtain concentration-sensitive images of the sample, which would reveal unambiguously any phase separation.

With this in mind, we prepared a sample that had a nominal composition of 3 MPM at 230 K and cooled it to 200 K. This composition was at one extreme of the proposed phase-separation region;[23] therefore, we did not expect to observe phase separation at this composition. We slowly cryopumped the ammonia gas from the sample back into the gas rig. By imaging this sample in real time, we were able to monitor for the onset of liquid−liquid phase separation in the Rb−NH_3 system. After the interface between the two liquids was identified (bubbling was observed to occur at this interface), the cryopumping was stopped and the phase separation was studied. A calculation of the sample concentration at this point gives a value of ∼8 MPM. This represents an upper concentration limit. The vapor pressure above the sample was ∼0.12 bar. A typical X-ray snapshot image is shown in Figure 1, along with a color interpretation, to aid the reader. The height of the sample, which is illuminated in the right-hand image, is ∼3 mm. This is deduced as only one change in the cell thickness can be seen, as shown by the thin horizontal line in the upper phase crossing the image at the top of the bubbles. Each step in the cell has a height of 3 mm, and no others are distinguishable in the image.

The observed phase separation is confirmed in Figure 2, in which the ratio of the transmitted beam intensity to incident beam intensity ($I(E)/I_0(E)$) is plotted as a function of sample cell height. By moving the sample cell ∼2 mm (from a distance of ∼17 mm to a distance of 18.95 mm) through the fixed-energy X-ray beam, the change from a metallic to a nonmetallic liquid is identified by the change in the sample absorption on crossing the interface. To these figures, we must add a brief description of the dynamic nature of the internal meniscus. At the interface between the concentrated (metallic) and dilute (nonmetallic) liquids, we observed the continuous formation of ammonia bubbles. As these bubbles grow, they rise from the interface and suddenly collapse as they reach the upper liquid surface. However, they do this *without* disturbing the external meniscus. Because of the long-term stability of our sample, and the low beam intensity during imaging, we do not believe that this behavior is caused by thermal gradients. In fact, because the

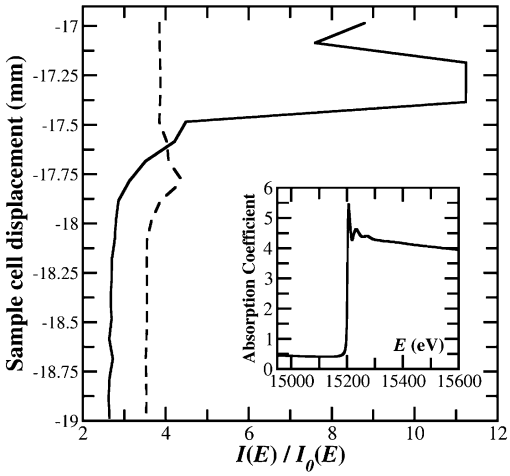

Figure 2. Ratio of the intensity of transmitted light to incident light through the two-phase solution, shown in Figure 1, as a function of the height of the sample container, relative to its location in the cryostat. Data are presented for photon energies of 15.3 keV (above the Rb K-edge absorption, solid curve) and 15.1 keV (below the Rb K-edge absorption, broken curve). Data were collected about the interface of constant sample thickness, i.e., below the step that is present in Figure 1. The regions of large and small intensity relate to the gold and blue regions of Figure 1, respectively. Inset shows the Rb K-edge absorption jump at ∼15.2 keV, and the EXAFS signal, for the (dilute) nonmetallic solution at 200 K, measured using a cell thickness of 1 mm.

dilute phase resides *underneath* the concentrated phase in this system, ammonia molecules that are diffusing upward must form a vapor as they cross the interface. In general, this is consistent with the vapor differences that have been observed between dilute and concentrated metal−ammonia solutions in which the vapor pressure decreases with metal concentration. In particular, this is supported for the Rb−NH_3 system in the work of Marshall, who reported the increase of the vapor-pressure reduction ($\Delta P/P_0$), relative to that of pure ammonia, with increasing metal content for Rb−NH_3 solutions at 238 K.[29]

At 200 K, the presence of bubbles that move from the interface into the upper phase prevented us from collecting a homogeneous EXAFS pattern. However, by cooling the sample, we confirmed that freezing occurs at 190 K. The sample was warmed slowly and began to melt at ∼193 K. Our intention was to examine the concentrated region; however, again, the sample bubbled in this region.

The observed Rb K-edge absorption for the dilute nonmetallic solution occurs at ∼15.2 keV, which is a value that is similar to that found in this study for Rb_2O. The position of the absorption edge is sensitive to the electronic environment of the absorbing species (see, for example, the work of Cramer and co-workers in the study of aqueous Mo ions in different oxidation states[30]). Thus, our results indicate that the valence state of Rb in both the solid oxide and the metal−amine solution are the same, i.e., +1. The edge energy E_0 was refined in the GNXAS analysis procedure.

In Figure 3, the calculated EXAFS signal ($\chi_m(k)$) obtained using the GNXAS suite of programs is shown, together with the EXAFS signal measured from a pellet of solid Rb_2O at room temperature (∼293 K). The total modeled $\chi_m(k)$ parameter is a linear contribution of three individual two-body correlations ($\gamma_2(k)$) that result from the nearest-neighbor Rb−O correlation at 2.92 Å and the first two Rb−Rb correlations, at 3.37 and 4.78 Å.[27] The individual two-body contributions are also shown. These correlations are associated with the corresponding coordination numbers of $n_{Rb-O} = 4$, $n_{Rb-Rb} = 6$, and $n_{Rb-Rb} =$

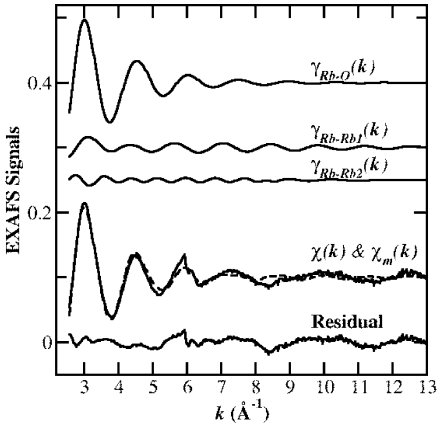

Figure 3. Calculated individual two-body contributions $\gamma_{Rb-O}(k)$ and $\gamma_{Rb-Rb}(k)$ and their sum $\chi_m(k)$, shown together with the measured $\chi(k)$ for solid Rb_2O at 293 K. The difference between the two $\chi(k)$ values is shown by the residual function.

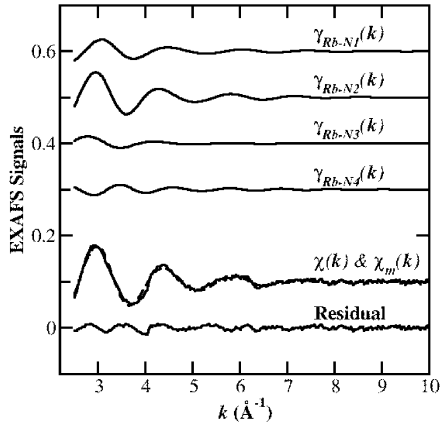

Figure 4. Calculated individual two-body contribution $\gamma_{Rb-N}(k)$, and their sum $\chi_m(k)$, shown together with the measured $\chi(k)$ values for the nonmetallic $Rb-NH_3$ solution at 200 K. The difference between the two $\chi(k)$ values is shown by the residual function.

12. Fair agreement is observed between the calculated and experimental data over the measured k-range.

In calculating the individual $\gamma_2(k)$, the parameter S_0^2 for the Rb_2O reference sample was determined. It was allowed to vary within a range of 0.7−1.0 in the fitting procedure for this sample. A value of 0.809 was obtained from the GNXAS fitting program, which is within the expected range of 0.8−1.[26] This parameter is a phenomenological component that provides a uniform reduction of the theoretical EXAFS signals:

$$\chi_m(k) = S_0^2 \sum \gamma_n(k) \tag{4}$$

where $n = 2$ in this study.

It is well-known that, above the Rb K-edge absorption, electron−electron interactions within the absorbing atom result in multielectron excitations that appear as absorption edges or resonances in the EXAFS spectrum. A prominent feature arises from the double-electron excitation [1s3d]4d that occurs at ∼130−140 eV above the edge.[31] In the data analysis procedure, this feature was treated as a "smooth step" and fitted using a smoothly varying function over the region of excitation.[26]

We turn our attention to $Rb-NH_3$ solutions, in which, for the data analysis, the values of $S_0^2 = 0.809$ and $E_0 = 15.201$ keV obtained for Rb_2O were used for the metal solutions. The individual contributions (γ_2), calculated for the first four distinct Rb−N correlations in crystalline $RbND_2$, were used to model the experimentally determined EXAFS signal for the nonmetallic $Rb-NH_3$ solution at 200 K. In reference to the proposed phase diagram,[23] the composition of this solution lies in the region of 3−4 MPM. These individual correlations are shown in Figure 4, with their total contribution $\chi_m(k)$, the measured contribution $\chi(k)$, and the residual function. The EXAFS signals $\gamma_2^{(1)}(k)$,$\gamma_2^{(2)}(k)$,$\gamma_2^{(3)}(k)$, and $\gamma_2^{(4)}(k)$ are associated with the first four distinct nearest-neighbor Rb−N correlations, which occur at 2.92, 3.03, 3.38, and 3.51 Å, respectively, in crystalline $RbND_2$, yielding coordination numbers of $n_{Rb-N} = 1, 2, 2$, and 1.[28] In the fitting procedure, the distances and coordination numbers associated with these correlations were allowed to vary from the crystalline compound. The best fit to the measured EXAFS signal was determined by initially setting the coordination numbers of the four generated Rb−N correlations in the input file to the fitting program FITHEO[26] to values of 0.95, 2.40, 2.39, and 0.70, respectively. A deviation of ±0.01 was applied to these coordination numbers. The output from the fitting program yielded the modeled $\chi_m(k)$ parameters that comprised

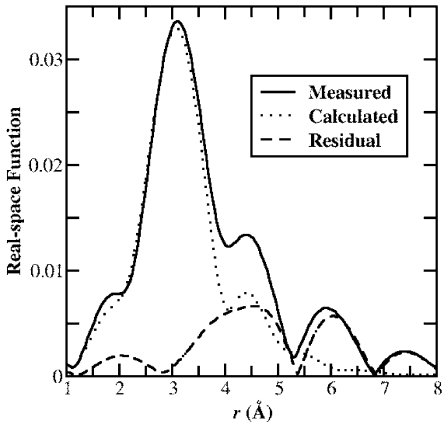

Figure 5. Fourier transforms of the measured and calculated EXAFS signals $\chi(k)$ and $\chi_m(k)$ for the nonmetallic $Rb-NH_3$ solution at 200 K are shown, as denoted by the unbroken and dotted curves, respectively. The residual function is given by the dashed curve. For all sets, a phase shift of ∼0.9 Å has been applied, as deduced from the Rb_2O reference sample.

the individual $\gamma_2(k)$ parameters which corresponded to Rb−N correlations centered at 2.91, 3.00, 3.36, and 3.51 Å, with final coordination numbers of $n_{Rb-N} = 0.94$, 2.41, 2.39, and 0.70, respectively. Hence, an average total coordination number of $n_{Rb-N} \approx 6.4$ is obtained. The Fourier transform of the measured and modeled EXAFS signals are shown together with the residual function in Figure 5. Our findings that Rb is ∼6-fold solvated by NH_3 molecules over the range of 2.9−3.5 Å, with the main peak centered at ∼3.1 Å, is not unexpected. This is consistent with the findings of Acrivos and co-workers, who identified the existence of the ionic species $Rb(NH_3)_6^+$ in $Rb-NH_3$ solutions at concentrations above and below the metal−nonmetal transition, with a nominal Rb−N distance on the order of 3 Å.[19] Furthermore, in determining the compressibility of metal−ammonia solutions, a similar solvation number of 6 was obtained for solutions that contained rubidium's neighbor, potassium.[32] Octahedral coordination of potassium by ammonia, with a K−N average distance of 2.85 Å, has been inferred from recent neutron diffraction experiments.[11]

Conclusions

The phase behavior and microscopic structure of liquid rubidium−ammonia ($Rb-NH_3$) solutions have been measured

below the consolute temperature (T_C), using the technique of extended X-ray absorption fine structure (EXAFS). Furthermore, the use of an X-ray video camera provides the first direct evidence for liquid−liquid phase separation of metallic and nonmetallic Rb−NH_3 solutions. Our real-time X-ray imaging provides an extraordinary glimpse of the dynamic nature of the interior liquid−liquid interface, from which bubbles of ammonia vapor "boil" without disturbing the external meniscus. We attribute this behavior to the fact that, in Rb−NH_3, the volume occupied by the solvated excess electrons ensures that the concentrated (metallic) solution is *less* dense than the dilute (nonmetallic) solution. Analysis of the EXAFS structure measured above the Rb K-edge absorption at ∼15.2 keV shows that, in dilute (nonmetallic) solutions, the cation is weakly solvated by ∼6.4 NH_3 molecules, at distance of 2.9−3.5 Å. The location of the K-edge absorption for our solution is comparable to that measured for solid rubidium oxide (Rb_2O), which is consistent with the valency of Rb being +1 in our solution. We therefore infer that Rb−NH_3 solutions are likely to be of future interest as the weakly structured limit of phase-separating metal−ammonia systems. We conclude by highlighting the pressing need for studies of critical fluctuations in this system: Does one observe the critical exponent crossover that is found in more-structured systems? In this context, there is also the likelihood that the deuterated rubidium−ammonia (Rb−ND_3) system will show an ∼10 K elevation of the T_C value, as is the case for deuterated lithium−ammonia and sodium−ammonia systems (Li−ND_3 and Na−ND_3, respectively).[33] Indeed, this raises the intriguing possibility that isotope-driven liquid−liquid phase separation would be observed in Cs−ND_3.

Acknowledgment. The authors are indebted to Ralf Weigel, Sebastian Pasternak, and Harald Müller for their invaluable help with the EXAFS experiments. Our thanks are extended to Adraino Filipponi (L'Aquila) for help with setting up the GNXAS analysis package. J.C.W. would like to thank Christopher E. Anson (Karlsruhe) and Piers Buchanan (King's College London) for helpful discussions concerning the crystal structures and data analysis, respectively. The stimulating conversations and encouragement of Peter P. Edwards (Birmingham University) are gratefully appreciated, as is the financial support of the EPSRC.

References and Notes

(1) Edwards, P. P. *J. Supercond.* **2000**, *13*, 933.
(2) Thompson, J. C. *Electrons in Liquid Ammonia*; Clarendon Press: Oxford, U.K., 1976.
(3) Edwards, P. P. *Adv. Inorg. Chem. R.* **1982**, *25*, 135.
(4) Damay, P.; Leclerq, F.; Chieux, P. *J. Phys. Chem.* **1984**, *88*, 3734.
(5) Damay, P.; Leclerq, F.; Chieux, P. *Phys. Rev. B* **1989**, *40*, 4696.
(6) Wasse, J. C.; Hayama, S.; Skipper, N. T.; Fisher, H. E. *Phys. Rev. B* **2000**, *61*, 11993.
(7) Burns, C. A.; Platzman, P. M.; Sinn, H.; Alatas, A.; Alp, E. E. *Phys. Rev. Lett.* **2001**, *86*, 2357.
(8) Burns, C. A.; Giura, P.; Said, A.; Shukla, A.; Vankó, G.; Tuel-Benckendorf, M.; Isaacs, E. D.; Platzman, P. M. *Phys. Rev. Lett.* **2002**, *89*, 236404.
(9) Hayama, S.; Skipper, N. T.; Wasse, J. C.; Thompson, H. *J. Chem. Phys.* **2002**, *116*, 2991.
(10) Thompson, H.; Wasse, J. C.; Skipper, N. T.; Hayama, S.; Soper, A. K.; Bowron, D. T. *J. Am. Chem. Soc.* **2003**, *125*, 2572.
(11) Wasse, J. C.; Hayama, S.; Skipper, N. T.; Benmore, C. J.; Soper, A. K. *J. Chem. Phys.* **2000**, *112*, 7147.
(12) Wasse, J. C.; Hayama, S.; Masmanidis, S.; Stebbings, S. L.; Skipper, N. T. *J. Chem. Phys.* **2003**, *118*, 7486.
(13) Tongraar, A.; Hannongbua, S.; Rode, B. M. *Chem. Phys.* **1997**, *219*, 279.
(14) Kerdcharoen, T.; Rode, B. M. *J. Phys. Chem. A* **2000**, *104*, 7073.
(15) Kraus, C. A. *J. Am. Chem. Soc.* **1907**, *29*, 1557.
(16) Pitzer, K. S. *J. Am. Chem. Soc.* **1958**, *80*, 5046.
(17) Mott, N. F. *Philos. Mag.* **1961**, *6*, 287.
(18) Edwards, P. P.; Sienko, M. J. *J. Am. Chem. Soc.* **1981**, *103*, 2967.
(19) Acrivos, J. V.; Hathaway, K.; Robertson, A.; Thompson, A.; Klein, M. P. *J. Phys. Chem.* **1980**, *84*, 1206.
(20) Quémerais, P.; Raimbault, J.-L.; Fratini, S. *J. Phys. IV* **2002**, *12*, 227.
(21) Ogg, R. A., Jr. *Phys. Rev.* **1946**, *69*, 243.
(22) Shannon, R. D. *Acta Crystallogr., Sect. A: Cryst. Phys., Diffr., Theor. Gen. Crystallogr.* **1974**, *32*, 751.
(23) Sharp, A. C.; Davis, R. L.; Vanderhoff, J. A.; LeMaster, E. W.; Thompson, J. C. *Phys. Rev. A* **1971**, *4*, 4.
(24) Filipponi, A. *J. Phys.: Condens. Matter* **2001**, *13*, R23.
(25) Filipponi, A.; Borowski, M.; Bowron, D. T.; Ansell, S.; Di Cicco, A.; De Panfilis, S.; Itiè, J.-P. *Rev. Sci. Instrum.* **2000**, *71*, 2422.
(26) Filipponi, A.; Di Cicco, A.; Natoli, C. R. *Phys. Rev. B* **1995**, *52*, 15122. Filipponi, A.; Di Cicco, A. *Phys. Rev. B* **1995**, *52*, 15135. Filipponi, A.; Di Cicco, A. *Task Q.* **2000**, *4*, 575.
(27) Helms, A.; Klemm, W. Z. *Anorg. Allg. Chem.* **1939**, *242*, 33.
(28) Bohger, P.; Zeiske, T.; Jacobs, H. Z. *Anorg. Allg. Chem.* **1998**, *624*, 364.
(29) Marshall, P. R. *J. Chem. Eng. Data* **1962**, *7*, 399.
(30) Cramer, S. P.; Eidem, P. K.; Paffet, M. J.; Winkler, J. R.; Dori, Z.; Gray, H. B. *J. Am. Chem. Soc.* **1983**, *105*, 799.
(31) De Panfilis, S.; Di Cicco, A.; Filipponi, A.; Comez, L.; Borowski, M. *J. Synchrotron Rad.* **2001**, *8*, 764. Li, G.; Bridges, F.; Brown, G. S. *Phys. Rev. Lett.* **1992**, *68*, 1609.
(32) Schroeder, R. L.; Thompson, J. C. *Bull. Am. Phys. Soc.* **1968**, *13*, 397.
(33) Katsumoto, M.; Damay, P. *J. Phys. Chem.* **1975**, *79*, 2928.